Imaging inflammation of the pancreatic islets in type 1 diabetes

Maria C. Denis*†, Umar Mahmood‡, Christophe Benoist*†, Diane Mathis*†§, and Ralph Weissleder‡

*Section on Immunology and Immunogenetics, Joslin Diabetes Center, 1 Joslin Place, Boston, MA 02215; †Department of Medicine, Brigham and Women's Hospital, Harvard Medical School, 75 Francis Street, Boston, MA 02115; and ‡Center for Molecular Imaging Research, Massachusetts General Hospital, Harvard Medical School, Building 149, 5406 13th Street, Charlestown, MA 02129

Contributed by Diane Mathis, June 17, 2004

Type 1 diabetes is the clinical manifestation of aberrant leukocytic infiltration of the pancreatic islets; it is usually diagnosed only very late in disease progression, after the critical autoimmune phenomena have mostly played out. A noninvasive means of directly monitoring the evolution of islet infiltrates would have important research and clinical applications. We have exploited fluorescence and MRI of long-circulating magnetofluorescent nanoparticles to visualize microvascular leakage, as an indicator of inflammation, in pancreata of mouse models of type 1 diabetes *ex vivo* or *in vivo*. We could detect the onset and evolution of insulitis *in vivo* and in real time, permitting us to study the natural history of diabetes in individual animals.

Type 1 diabetes (T1D) results from T lymphocyte attack on the insulin-producing β cells of the islets of Langerhans of the pancreas. Disease unfolds through the following two main stages: the occult phase, termed insulitis, when a mixed population of leukocytes invades the islets, promoting β cell death; and the overt phase, diabetes, when the bulk of β cells have been destroyed and the pancreas can no longer produce sufficient insulin to control blood glucose levels.

A major hindrance to the study of T1D is that its overt manifestation signifies that most of the islet β cells have already been destroyed and that the preceding (autoimmune) processes have already played out. Experimentally, in animal models, this late diagnosis engenders difficulties in charting the early events and unraveling their underlying mechanisms, especially given that individual animals exhibit significant scatter in disease parameters and variability in disease course. Clinically, diagnosis at such a late stage creates problems for providing effective therapy because, by that time, options for disease reversal are already severely limited and analogous disease heterogeneity precludes earlier "blind" intervention.

Thus, much effort has been devoted to identifying markers that indirectly signal at least the major landmarks of T1D progression. So far, the best indicator of islet inflammation has been serum titers of autoantibodies directed against a defined set of β cell antigens (1). Although monitoring autoantibody titers has significant predictive value at the population level, a noninvasive means of directly following disease progression *in vivo* would have important applications. For example, images of the insulitic lesion may facilitate difficult diagnoses (e.g., of late autoimmune diabetes of adults), should enable disease monitoring during its natural course or pursuant to immunomodulatory interventions, and may provide forewarning of pancreas graft rejection. Ultimately, such images may allow the detection of early autoimmune processes in genetically at-risk individuals at the earliest stages.

We anticipated that recently developed strategies for noninvasive imaging of the microvasculature might provide powerful means to attack this problem. Modifications of the pancreatic microvasculature are likely to accompany the initiation and progression of T1D. Alterations in vascular parameters, such as transient vasoconstriction, vasodilation, increased blood flow, and vascular leakage, are necessary preludes to inflammation, and they help to orchestrate the influx of diverse cell types (2). Not surprisingly, changes in intraislet vasculature precede streptozotocin-induced insulitis (3–6) and vascular swelling and modifications of endothelial cell morphology in the paraislet region signal impending insulitis in nonobese diabetic (NOD) mice (7). In both of these diabetes models, and other models, increased blood flow and edema ensue (6, 8, 9). Such modifications might be detectable by certain of the powerful new methodologies for imaging the microvasculature in rodents and humans described recently (10).

One highly successful approach has been the use of novel biocompatible nanomaterials as vascular probes for fluorescence (11) or MRI (12). Here, we use long-circulating magnetofluorescent nanoparticles (CMFN) with vascular half-lives of >10 h as probes of microvascular changes accompanying inflammation. The nanoparticles contain a small, monocrystalline, superparamagnetic iron oxide core, which exhibits strong magnetic behavior detectable by high-resolution MRI. The 3-nm core is surrounded by a dense, modified-dextran coating that diminishes the immunogenicity of the assembled particles (25 nm) and substantially enhances their half-life in circulation. A further sophistication has been the generation of coatings modified with "tags," such as fluorochromes or radioisotopes, thereby permitting detection by additional imaging techniques (13). Importantly, the resultant materials are brightly fluorescent and highly magnetic. These vascular probes also have other attractions, such as their nontoxicity, nonimmunogenicity, long circulation time, and promising performance in clinical trials. Indeed, MRI of related materials was recently applied with great success to patients with prostate cancer, enabling visualization of small and otherwise undetectable lymph-node metastases (14). An analogous approach applied to T1D patients might prove to be very powerful. Here, we apply CMFN to image inflammation of pancreatic islets in mouse models of T1D *ex vivo* or *in vivo*.

Methods

Mice. NOD/Lt, Eα16/NOD, NOD-RAG$^{-/-}$, BDC2.5/NOD, BDC2.5/B6.H-2$^{g7/g7}$, and BDC2.5/NOD-RAG$^{-/-}$ mice were bred in our animal facility under specific-pathogen-free conditions. Diabetes was monitored by measuring glucose in the urine (Diastix, Bayer, Elkhart, IN) and was confirmed by measuring blood glucose levels (Glucometer Elite, Bayer).

Histology and Insulitis Scoring. Mouse pancreata were fixed overnight in 10% neutral-buffered formalin (Sigma). Thin sections of paraffin-embedded pancreata were examined after hematoxylin–eosin staining. Multiple sections were taken from at least three different levels. "Insulitis" refers to lesions with a clear and often extensive islet infiltrate exhibiting direct lymphocyte–β cell contact but with an obvious demarcation of the infiltrate and relatively healthy β cells. "Aggressive insulitis" refers to an extensive infiltrate, where lymphoid cells invade the entire islet, intermingling with endocrine cells, with extensive signs of β cell damage.

Abbreviations: T1D, type 1 diabetes; NOD, nonobese diabetic; CMFN, long-circulating magnetofluorescent nanoparticles; DTZ, dithizone; Hst, Hoechst; TCR, T cell receptor; tg, transgenic; ROI, regions of interest; MFI, mean fluorescence intensity.

§To whom correspondence should be addressed. E-mail: dm@joslin.harvard.edu.

www.pnas.org/cgi/doi/10.1073/pnas.0404307101

Imaging Probes. The CMFN used in this study consisted of a core of superparamagnetic iron oxide and a crosslinked dextran coating with amino groups to which Alexa-488 fluorochrome (Molecular Probes) was attached (15). On average, each monocrystalline nanoparticle had 24 fluorochromes, a mean particle size of 25 nm (as determined by laser light scattering), an R1 of 20 $mM \cdot sec^{-1}$, and an R2 of 45 $mM \cdot sec^{-1}$. For selected MRI studies, we also used a previously described and related material (MION-47) with identical magnetic and biological properties (16, 17).

Islets were revealed by staining with diphenylthiocarbazone (dithizone, DTZ) (Sigma), which can be detected by confocal microscopy because of its autofluorescence properties in the red channel. Nuclei were demarkated by staining with Hoechst (Hst) 33342 dye (Calbiochem).

Flow Cytometry. Animals were perfused with 15 ml of PBS containing 1 unit/ml heparin (Sigma–Aldrich), and their pancreata were digested with collagenase P (Roche Molecular Biochemicals) at 37°C for 20 min. Digested material was pipetted vigorously and filtered in cold wash buffer containing 5 mM EDTA. Bulk organ suspensions were stained for multicolor flow cytometry with the antibodies listed in *Supporting Methods*, which is published as supporting information on the PNAS web site.

Confocal Microscopy. Routinely, animals were i.v. injected with 10 mg of Fe per kg of CMFN (CLIO)/Alexa-488, and pancreata were excised for imaging after 5 min or 24 h. DTZ and Hst counterstaining, perfusion, and fixation procedures varied according to the experiment, as detailed in the figure legends. Additional details of the imaging of islets in whole pancreata are given in *Supporting Methods*.

MRI. T2 measurements were performed with an 8.5-tesla microimaging system (DRX-360, Bruker BioSpin MRI, Karlsruhe, Germany) and reported as R2 relaxation rates of tissue ($R2 = T12^{-1}$) by standard procedures, as described in *Supporting Methods*.

Statistical Analysis. Data were analyzed by using a two-tailed and two-sample unequal variance Student's *t* test. Values of $P \leq 0.05$ were considered significant.

Results

Our ultimate goal is to develop a means of noninvasively imaging inflammation of the pancreatic islets in humans with, or at risk of developing, T1D. An important milestone would be establishment of "proof-of-principle" in a murine T1D model. We have chosen the BDC2.5 T cell receptor (TCR) transgenic (tg) mouse model for this purpose because insulitis in these animals is more synchronous and homogenous and, therefore, more predictable than it is in the standard NOD model (18). BDC2.5 TCR tg mice carry the rearranged TCR genes from a diabetogenic $CD4^+$ T cell clone isolated from a NOD mouse and reactive to an islet β cell antigen presented by the MHC class II molecule A^{g7}. Consequently, these animals have a T cell repertoire that is highly skewed for the transgene-encoded, β cell-reactive specificity. All animals exhibit insulitis abruptly at 2–3 wk of age, but the rate and penetrance of diabetes development varies according to the genetic background (19). We hypothesized that CMFN would permit convenient analysis of the pancreatic microvasculature in BDC2.5 TCR tg mice and that detectable changes in the islet blood vessels would accompany the onset and/or progression of insulitis.

***Ex Vivo* Visualization of Microvascular Leakage in the BDC2.5 Model.** We first sought to image leakage from microvessels associated with the pancreatic islets. Work on other systems has established that shortly after i.v. injection, CMFNs remain largely within the blood vessels, permitting visualization of the vascular bed; by 24 h after administration, the nanoparticles have had time to leak into the surrounding tissue and, thereby, can signal changes in vascular permeability (16, 20). Initially, we used *ex vivo* microscopic visualization of fluorescently labeled (Alexa-488) CMFN in excised pancreata. Routinely, animals were injected i.v. with CMFN (green) and then injected 24 h later with DTZ or Hst dyes to stain the islets (red) or nuclei (blue), respectively. Pancreata were removed 5 min later, and the fluorescent signals were visualized by confocal microscopy. Negative-control animals, devoid of insulitis, were routinely NOD-$RAG^{-/-}$ or Eα16/NOD mice (see below for description).

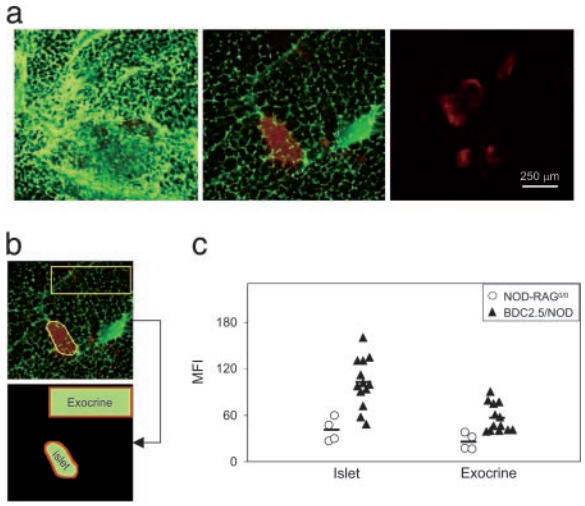

Fig. 1. *Ex vivo* confocal microscopic imaging of microvascular leakage accompanying insulitis in BDC2.5 TCR tg mice. We injected 4-wk-old female BDC2.5/NOD or NOD/$RAG^{-/-}$ mice with 10 mg/kg CMFN diluted with PBS to 150 μl or with PBS only. Twenty-four hours later, they were i.v. injected with 25 mg/kg DTZ, and, after 5 min, the whole pancreas was removed and imaged by confocal microscopy using a $\times$10 objective. Islets were identified by DTZ staining (red), and signal from the CMFN probe (green) was visualized and quantitated. (*a*) CMFN probe accumulation, reflective of microvascular leakage, as an accompaniment to islet infiltration. Images are representative of islets from at least three animals of each type in each condition. (*b*) Procedure to quantitate probe accumulation. Custom-designed image-analysis software was used to measure the MFI of CMFN over ROI that represent islets (identified by DTZ staining) or exocrine tissue (an area selected as distinct from islets and major vessels). (*c*) Quantitative comparison of insulitic and noninsulitic pancreata. We took 13 4-wk-old BDC2.5/NOD and age-matched NOD-$RAG^{-/-}$ animals. Symbols represent the MFI of individual animals calculated as the average MFI of all of the islets (4–10) acquired per animal. Bar represents the average value.

An accumulation of the CMFN probe was evident in the pancreas images derived from insulitic 4-wk-old BDC2.5/NOD mice (Fig. 1*a*). Strong green fluorescence surrounded the red-stained islets of these animals (*Left*), in contrast to the weak green fluorescence in islet regions of age-matched, noninsulitic NOD-$RAG^{-/-}$ controls (*Center*) and the absence of autofluorescence in analogous regions of control, PBS-injected animals (*Right*). The weak fluorescence associated with normal islets can probably be attributed to a slight amount of leakage from the fenestrated islet microvasculature (21). Custom-designed image analysis software was used to integrate CMFN fluorescence in regions of interest (ROI) encompassing paraislet and extraislet areas of the pancreas images (Fig. 1*b*; detailed in *Methods*). These analyses revealed significant accumulation of the probe in the insulitic pancreata of BDC2.5/NOD mice, most strikingly in regions immediately surrounding the islets ($P = 0.0003$) but also spilling over into exocrine regions ($P = 0.003$) (Fig. 1*c*).

To explore the location of CMFN probe accumulation in insulitic pancreata, we performed a perfusion experiment by flushing PBS and then formalin through the left ventricle of the heart just before

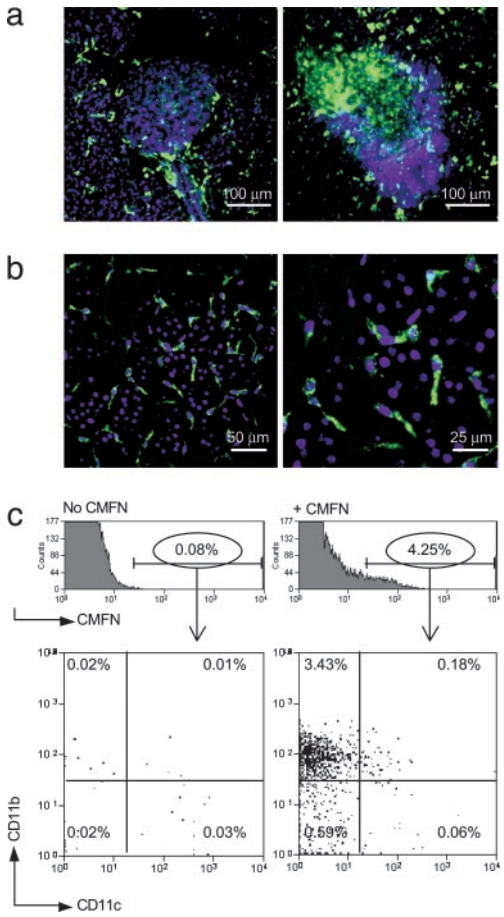

Fig. 2. CMFN probe uptake by macrophages in the vicinity. We injected 4-wk-old female BDC2.5/NOD and Ea16/NOD mice with CMFN, as described in the legend to Fig. 1. Twenty-four hours later, animals were anesthetized and i.v. injected with 25 mg/kg Hst to stain nuclei, and after 5 min, they were perfused through the left ventricle with PBS/heparin, followed by 5 ml of 10% neutral-buffered formalin. The pancreas was further fixed overnight in 10% neutral-buffered formalin. It was placed in glycerol-based mounting medium and kept for 1 wk until transparent enough to visualize. (*a*) A noninfiltrated vs. an infiltrated islet. Images are representative of those from at least two animals of each genotype. CMFN, green; Hst, blue. The mass of blue nuclei corresponds to lymphocytic infiltrate, as identified histologically. A ×25 objective was used. (*b*) Higher magnification. Images reveal the uptake of CMFN (green) by cells of macrophage-like morphology. Nuclei of infiltrating, mostly lymphoid, cells are stained blue with Hst. A ×40 objective was used. (*c*) Identification of the cellular repository by flow cytometry. A group of three 4-wk-old female BDC2.5/NOD mice was used per sample. One group was left uninjected, whereas the other group was i.v. injected with 10 mg/kg CMFN and was otherwise treated as described above except that no counterstain or fixative was administered. After perfusion, the pancreas was treated with collagenase, washed, and made into a single-cell suspension for staining. CMFN-positive cells were gated as shown in *Upper*, and staining by anti-CD11b and CD11c reagents is shown.

removal of the pancreas. The increase in green fluorescence in insulitic vs. noninsulitic pancreata was as evident after perfusion (Fig. 2*a* and data not shown), confirming that the signal originated from "leaked" probe. In addition, the appearance of the sections suggested that, when extravasated into the interstitium, the nanoparticles were taken up rapidly by cells in the neighborhood. These cells could be visualized by means of higher-magnification microscopy of pancreas tissue in which cell nuclei had been counterstained blue with Hst. The distribution of the cells suggested that they were participants in the leukocytic infiltrate, clumped in close association with the islets (Fig. 2 *a* and *b*). The morphology of the cells was consistent with their being macrophages or dendritic cells (Fig. 2*b*), as has been reported in studies on other systems (22). Indeed, cytofluorimetric analysis confirmed that the CMFN-labeled cells had a cell-surface phenotype ($CD11b^{+}11c^{-}$) that is characteristic of macrophages (Fig. 2*c*).

These data establish the usefulness of the CMFN probe for exploring the microvasculature of the pancreatic islets and demonstrate that insulitis is accompanied by an increase in probe accumulation. This concentration in extravessel regions probably results both from an increase in microvascular permeability, promoting probe leakage, and an influx of phagocytic macrophages, permitting probe up-take, and, thereby, inhibiting its diffusion.

Relationship Between CMFN Probe Accumulation and the Aggressiveness of the Insulitic Lesion. An obvious question that arises is how the accumulation of extravasated CMFN probe correlates with insulitis aggressivity. How does the fluorescent signal intensity change with the unfolding of the lesion? How is it influenced by the cellular participants of the lesion? Experiments designed to answer these questions exploited BDC2.5/NOD mice of various ages or with diverse genetic deficiencies. The protocol was the standard one described above.

Insulitis develops abruptly and synchronously at 2–3 wk of age in BDC2.5/NOD mice (23). This behavior was nicely "captured" by the CMFN probe as follows: an intense green signal surrounded the islets in images from 3-wk-old, but not 2-wk-old, animals (Fig. 3*a i* vs. *iv*). Such a difference was not observed on images from age-matched, noninsulitic NOD-$RAG^{-/-}$ animals (Fig. 3*a ii* vs. *v*) nor in the absence of probe (Fig. 3*a iii* vs. *vi*).

Next, we performed a quantitative kinetic analysis (Fig. 3*b*). Changes in CMFN accumulation occurred over time whether the mean fluorescence intensity (MFI) of individual islets or the average MFI for individual animals was plotted (Fig. 3*b i* and *ii*). In the case of NOD-$RAG^{-/-}$ mice, which are devoid of lymphocytes and consequently of insulitis, MFI values dropped steadily from 2–15 wk of age, probably reflecting maturation of the vascular architecture, closing the remaining gaps between endothelial cells and establishing tight junctions (24). For pancreata from BDC2.5/NOD mice, MFIs were minimal at 2 wk of age, indistinguishable from those of NOD-$RAG^{-/-}$ controls of the same age. There was a sharp increase in BDC2.5/NOD MFIs at 3 wk, which maximized at 4 wk. By 6 wk of age, MFIs had dropped somewhat and remained steady to 15 wk but were always significantly higher than the analogous values derived from age-matched NOD-$RAG^{-/-}$ controls. There turned out not to be a simple linear relationship between the degree of insulitis and level of fluorescence intensity (Fig. 3*biii*). In younger mice (<4 wk), the MFI did increase along with infiltration, but a later decline occurred while insulitis was still very evident.

Genetic variants of the NOD and BDC2.5/NOD models permit one to explore the influence of the cellular composition of the lesion on CMFN probe accumulation. NOD-$RAG^{-/-}$ mice lack α/β T and B lymphocytes, and consequently, they do not develop insulitis (19); Eα16/NOD animals have seemingly normal α/β T and B lymphocyte compartments but are protected from insulitis, likely because of a greater number or activity of regulatory T cells (25). These two NOD variants are similar, then, in being noninsulitic but differ in their repertoire of lymphocytes. Significant accumulation of the CMFN probe was observed in the pancreas of 4-wk-old individuals in neither case, reflecting an intact microvasculature (shown in Fig. 3*c i* and *ii*; quantitated in Fig. 3*di*).

The appearance of the islet infiltrates in young BDC2.5 TCR tg mice differs according to the genetic background (19). BDC2.5/NOD animals at 3–4 wk of age have a very extensive but innocuous lesion that circumscribes the β cell mass and seldom progresses to diabetes. Age-matched BDC2.5/B6.H-$2^{g7/g7}$ and BDC2.5/NOD-$RAG^{-/-}$ animals have more aggressive lesions, with activated leukocytes, dying β cells, and heavy intermingling between the two, resulting in a high penetrance of diabetes at a young age, being most

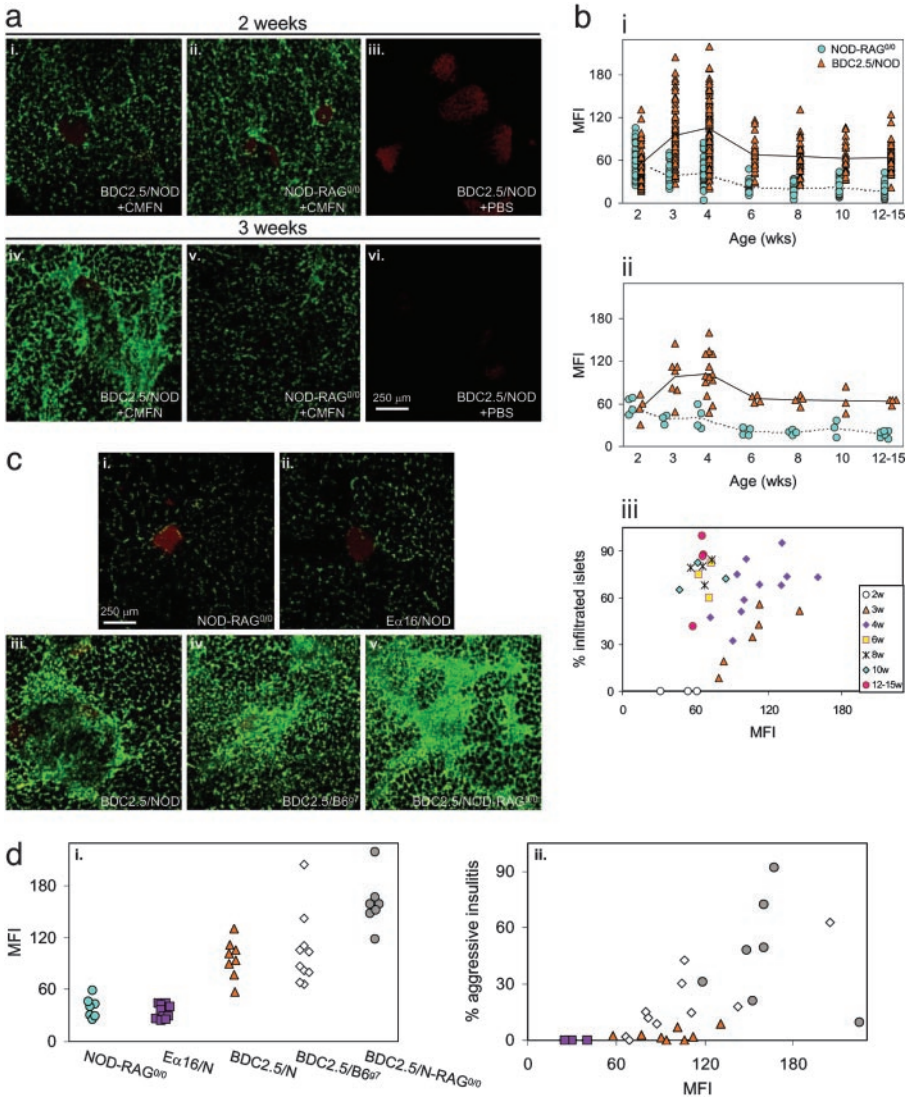

Fig. 3. More aggressive insulitis leads to more probe accumulation. (*a*) At initiation of insulitis. Two- or 3-wk-old female BDC2.5/NOD or NOD-RAG$^{-/-}$ mice were injected with CMFN (or PBS) and DTZ, and their pancreas were imaged *ex vivo*, as described in the legend to Fig. 1. A 10× objective is shown. (*b*) Through the evolution of insulitis. The procedures were the same as described above except that animals ranged in age from 2 to 15 wk. MFIs were calculated as described in the legends to Fig. 1 *b* and *c*. Symbols represent values for individual islets (*i*) or averages of all islet values for individual animals (*ii*). Average MFIs of CMFN signals for pancreata of individual animals were correlated with the fraction of the animal's islets that were infiltrated, which was assessed from hematoxylin–eosin (H&E)-stained sections of the same pancreas used for imaging. (*c* and *d*) According to the composition and appearance of the infiltrate. Pancreata were obtained from CMFN/DTZ-injected NOD variants protected from insulitis because of a lack of α/β T and B cells (*ci*) or to an augmentation of regulatory T cell numbers or activity (*cii*), or from CMFN/DTZ-injected BDC2.5 TCR tg mice on different genetic backgrounds, promoting greater insulitis aggressivity in the following order: BDC2.5/NOD (*ciii*) < BDC2.5/B6.H-2^{g7g7} (*civ*) < BDC2.5/NOD-RAG$^{-/-}$ (*cv*). Images were taken with a 10× objective. Images were quantitated and MFIs surrounding the islets plotted (*di*) and correlated with insulitis intensity revealed by H&E histological analysis (*dii*).

extreme in the latter strain (26). In all three cases, pancreas images showed strong accumulation of the CMFN probe, indicative of microvascular leakage (Fig. 3*c iii–v*), but quantitative analysis did reveal a clear increase in the MFI values with enhanced insulitis destructiveness and progression to diabetes (Fig. 3*di*). Overall, there was a strong correlation between the aggressivity of the lesion as measured histologically and the CMFN signal (Fig. 3*dii*). That the aggressivity of insulitis, rather than its simple extent, correlated with vascular leakage, and probe accumulation is consistent with the time course in BDC2.5/NOD mice (Fig. 3*b i* and *ii*); these animals show a less extensive but more aggressive insulitis at 3–4 wk of age, which then settles into a more abundant but less active lesion.

Clearly, the CMFN probe was able to portray the degree of insulitis aggressivity both during unfolding of the BDC2.5/NOD lesion through time and with the variably destructive lesions of NOD and BDC2.5 variants carrying different mutations or on different genetic backgrounds.

***Ex Vivo* Visualization of Microvascular Leakage in the NOD Model.** It was obviously of interest to compare the situation in NOD mice. Insulitis is less synchronous and florid in this more complex T1D model; routinely, it becomes evident at 6–8 wk of age but initiates and progresses with variable rapidity and severity in different individuals. NOD mice at ages of 2–15 wk were imaged with CMFN, as described above. The time-course curves for NOD mice (Fig. 4 *a* and *b*) were clearly different from those generated by using BDC2.5 animals (Fig. 3*b i* and *ii*). Whether one considers individual islets (Fig. 4*a*) or individual animals (Fig. 4*b*), the signals associated with the islets of NOD mice were essentially identical to those associated with NOD-RAG$^{-/-}$ islets at young ages. Significant differences show up only at the latest (12–15 wk) time point (Fig. 4 *a*, $P < 0.00001$, and *b*, $P = 0.0002$). Here, there was a clear relationship between probe accumulation and the extent of insulitis (Fig. 3*biii*). This observation is consistent with the much slower progression of insulitis in NOD mice, which may not "mature" as rapidly as it does in BDC2.5/NOD animals.

Thus, the CMFN probe also permits monitoring of insulitis progression in standard NOD mice, although the signal differential may be less impressive than with the BDC2.5 TCR tg model.

***In Vivo* Imaging.** The stage was now set for *in vivo* imaging of microvascular leakage as a noninvasive measure of insulitis progression. Because CMFNs are also highly magnetic, we next performed *in vivo* experiments to visualize them in orthopic pancreata by MRI, as might eventually be done in humans. We anesthetized 4-wk-old BDC2.5/NOD or age-matched negative-control Eα16/NOD mice, and a first, preinjection, MRI was acquired. The animals were then i.v. injected with CMFN and imaged a second

IMMUNOLOGY

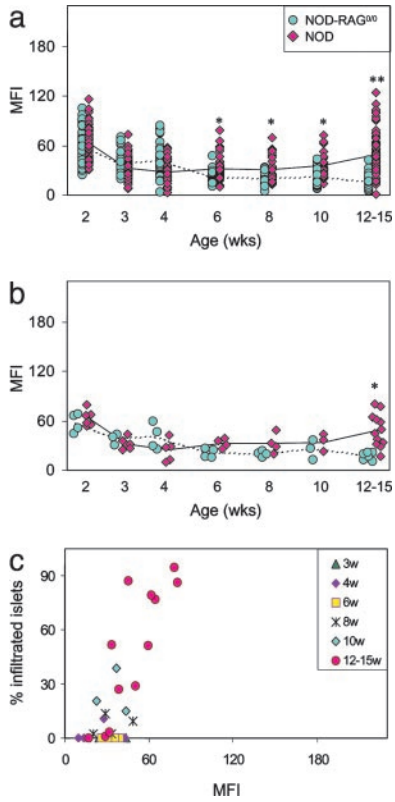

Fig. 4. *Ex vivo* imaging of leakage accompanying insulitis in NOD mice. (*a* and *b*) MFIs of CMFN signal associated with pancreatic islets of insulitic NOD vs. noninsulitic NOD-RAG$^{-/-}$ female mice. Insulitis becomes evident in NOD mice at 6–8 wk. Animals were injected and pancreata processed for *ex vivo* confocal microscopic imaging as described in the legend to Fig. 1. Values reflect signal over individual islets (*a*) or the average signal over all of an animal's 4–10 scored islets (*b*). $P \leq 0.005$ at 6–10 wk, and $P < 0.00001$ at 12–15 wk in *a*; and $P = 0.0002$ at 12–15 wk in *b*. (*c*) Correlation between the average MFIs of CMFN signal over the islets and the fraction of infiltrated islets in individual NOD mice sorted according to age. Values were calculated as described in the legend to Fig. 3*biii*.

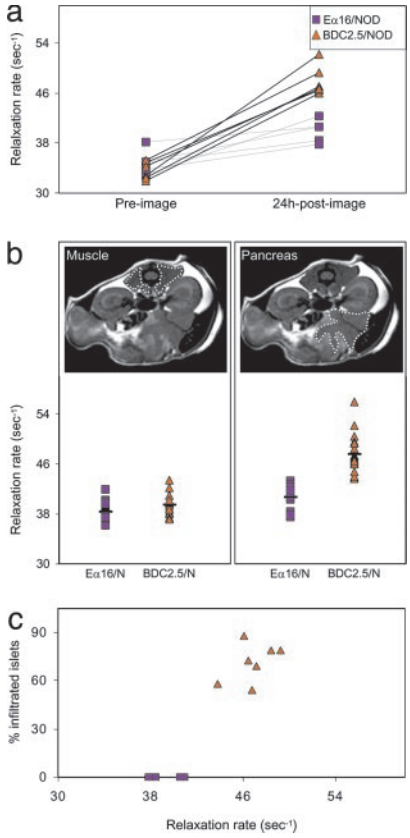

Fig. 5. *In vivo* visualization of infiltrated pancreata. We anesthetized 4-wk-old female insulitic BDC2.5/NOD or noninsulitic Eα16/NOD mice and immediately "preimaged" them by MRI; i.v. injected them with 40 mg/kg MION-47; and, after 24 h, anesthetized and "postimaged" them by MRI. ROI were drawn around different organs. (*a*) Comparison of preimage and 24-h postimage values for the two strains. Symbols represent values for individual pancreata, and their correlation is explained in *Methods*. *P* values were significantly different between the 24-h postimages of BDC2.5/NOD and Eα16/NOD mice ($P = 0.0001$) and the preimages and 24-h postimages of BDC2.5/NOD mice ($P < 0.00001$). (*b*) Parallel comparisons with muscle tissue. *Upper* shows delineation of ROIs, and *Lower* shows the values for muscle and pancreas. (*c*) Correlation between degree of islet infiltration, calculated as described in the legend to Fig. 3*biii*, and accumulation of MION probe.

time 24 h later. An ROI was drawn around the pancreas (e.g., Fig. 5*b*), and the signal in a 1-mm slice was quantitated as the reciprocal of the relaxation rate.

Preinjection values for pancreata from BDC2.5/NOD and Eα16/NOD mice were indistinguishable, and there was very little effect of the CMFN injection on the 24-h-postinjection figures for pancreata from Eα16/NOD animals (Fig. 5*a*), consistent with the minimal leakage seen by confocal values for pancreata from BDC2.5/NOD animals. However, the CMFN probe clearly modified the values at 24 h after injection for pancreata from BDC2.5/NOD animals. These divergences were specific to the pancreas because they were not observed in other tissues, such as muscle (Fig. 5*b*). In general, those animals with the highest pancreas values exhibited the most extensive insulitis, as scored histologically (Fig. 5*c*).

Next, we used this technique to follow the progression of insulitis in individual animals through time (Fig. 6), which was made possible by the noninvasive nature of MRI. There were some time-dependent changes in MRI intensity over time, and signals from muscle tissue were used for standardization. As we had seen on the population level, by visualizing paraislet accumulation of the CMFN probe in pancreata *ex vivo*, there was a significant concentration of MION in insulitic pancreata of 4-wk-old BDC2.5/NOD mice *vis a vis* the noninsulitic organ of age-matched Eα16/NOD controls ($P = 0.009$). However, this difference had largely disappeared by 6 wk of age. This evolution reflected well the decrease in microvascular leakage around the well established lesions.

Thus, we conclude that the evolution of insulitis in BDC2.5 TCR tg mice can be monitored noninvasively *in vivo* in real time by measuring leakage of the microvasculature using CMFN-enhanced MRI.

Discussion

MRI of CMFN probes has proven to be a powerful method of noninvasively visualizing vascular and cellular modifications associated with inflammation. For example, within 24 h after i.v. injection into humans or rodents, nanoparticles can extravasate from "leaky" vessels into the surrounding tissue and be engulfed by activated macrophages that have invaded the tissue. We hypothesized that such alterations in the microvasculature accompany the leukocyte infiltration of the pancreatic islets that is the hallmark of T1D, and that these modifications can be read out as CMFN accumulation in the pancreas. We exploited the relatively homogenous and synchronous BDC2.5 TCR tg mouse model of T1D to test this hypothesis, first by employing fluorescently tagged CMFN probes imaged *ex vivo* by confocal microscopy to optimize the methodology and then by using the magnetic properties of CMFN

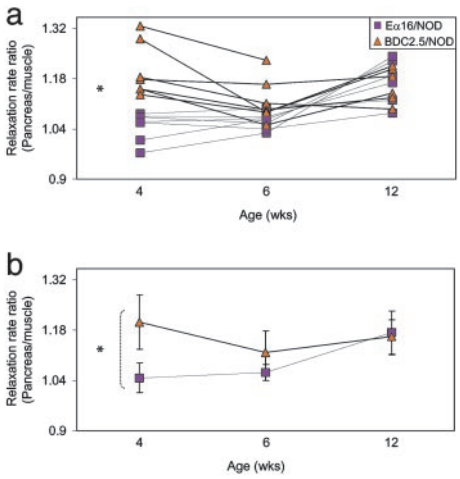

Fig. 6. A noninvasive, real-time longitudinal study of islet infiltration. Imaging of MION probe accumulation in organs of individual BDC2.5/NOD or Eα16/NOD female mice, as described in the legend to Fig. 5. Values reflect the ratio of relaxation rate measured over ROIs encompassing the pancreas and muscle. Values for individual animals (*a*) or average values for all individuals of each strain (*b*) are given.

to MRI *in vivo*. Indeed, we were able to noninvasively follow the initiation and progression of insulitis in BDC2.5 mice by MRI monitoring of CMFN probe accumulation *in vivo* in real time.

In general, there was a positive correlation between CMFN probe accumulation in the pancreas and insulitis aggressivity. However, the longitudinal study of insulitis evolution in BDC2.5/NOD mice generated a CMFN accumulation curve with an interesting shape: a sharp increase at 2–3 wk of age, a decrease at 4–6 wk, and little change to 15 wk. The punctual increase at 2–3 wk of age was exactly as expected, a nice reflection of the abrupt initiation of insulitis during this precise time window (23). The decrease at 4–6 wk likely correlates with maturation of the insulitic lesion in BDC2.5/NOD mice. Over this time period, the infiltrate becomes more organized, with an augmented frequency of small resting cells, and lymphoid cells segregate, with B lymphocytes congregating in follicle-like structures. This architecture, which is reminiscent of lesions in NOD mice subject to diabetes "reversal" by strong immunomodulation just after onset, appears to be less active than in the very first days of insulitis. CMFN accumulation at sites of inflammation signals at least the two following processes: an increase in probe extravasation, which could be due to an augmented vessel leakage, blood flow, and/or vessel density; and an increase in probe uptake, which might signal more or different phagocytic cells in the vicinity. Any of these parameters might change through evolution of the insulitic lesion in BDC2.5 mice. Indeed, 3D reconstruction of confocal images of pancreata from BDC2.5 animals perfused with heparinized PBS, then with CMFN probe plus fixative and immediately dissected, suggests a decrease in islet vessel diameter and density as disease unfolds (M.C.D., unpublished data). There have also been reports of changes in macrophages and/or dendritic cell populations through the evolution of insulitis in NOD mice, in particular in the 3- to 7-wk time window (27–29).

Nanoparticle-induced signal changes were less striking in the standard NOD model than in the more homogeneous and synchronous BDC2.5 TCR tg system. This divergence likely reflects the kinetic difference in the insulitic lesions of the two types of mice, the lower frequency of autoreactive T cells in the former promoting a more progressive onset of insulitis. Indeed, NOD mice become fully insulitic only by 12 wk of age, and the CMFN signal mimics well this time course. Alternatively, or in addition, it might be a reflection of qualitatively different lesions in the two cases, perhaps composed of divergent, or divergent ratios of, cell types, for example of phagocytic cells. Indeed, Rosmalen *et al.* (30) have reported that macrophage subsets defined on the basis of mAb markers participate differentially in the leukocytic infiltrates of BDC2.5 and NOD mice. Regardless, confocal microscopic imaging did reveal clear differences in the accumulation of CMFN probe in the infiltrated islets of older vs. younger NOD mice (Fig. 4), and preliminary studies have proved this finding to be true for MRI of the CMFN probe as well (M.C.D., unpublished data).

Thus, we have developed a means to noninvasively monitor the initiation and progression of insulitis in mouse models of T1D *in vivo* and in real time. This methodology will permit us, on an individual mouse basis, to correlate directly immunological and metabolic parameters with the evolution of the insulitic lesion, either during the natural unfolding of disease or subsequent to therapeutic intervention. Potentially, it may even allow prediction of whether and when overt diabetes will develop in the future. Given the published success and nontoxicity of CMFN probes in the human context (14), application of this methodology to T1D in patients may have great potential.

We thank E. Hyatt, C. Cahill, S. Kalogrianitis, G. Losyev, M. Takahashi, and E. Graves for their important technical contributions. This work was supported by National Institutes of Health Grants 5RO1DK059658 (to D.M. and C.B.), 2P30DK36836 and PO1AI54904 (to D.M., C.B., R.W., and U.M.), and P50CA86355 and R24CA92782 (to R.W.) and Joslin Diabetes and Endocrinology Research Center Core Grant 2P30DK36836-17. M.D. received National Institutes of Health National Research Service Award Individual Postdoctoral Fellowship 1F32-DK63886, and U.M. received an American Roentgen Ray Society Scholarship.

1. Eisenbarth, G. S., Moriyama, H., Robles, D. T., Liu, E., Yu, L., Babu, S., Redondo, M., Gottliev, P., Wegmann, D. & Rewers, M. (2002) *Autoimmun. Rev.* **1,** 139–145.
2. Pober, J. S. & Cotran, R. S. (1990) *Transplantation* **50,** 537–544.
3. Sander, S. & Jansson, L. (1985) *Virchows Arch.* **407,** 359–367.
4. Beppu, H., Maruta, K., Kurner, T. & Kolb, H. (1987) *Acta Endocrinol.* **114,** 90–95.
5. Martin, S., Kolb-Bachofen, V., Kiesel, U. & Kolb, H. (1989) *Diabetologia* **32,** 359–367.
6. Papaccio, G. (1993) *Histol. Histopath.* **8,** 751–759.
7. Papaccio, G., Latronico, M. V., Pisanti, F. A., Federlin, K. & Linn, T. (1998) *Autoimmunity* **27,** 65–77.
8. Carlsson, P.-O., Sandler, S. & Jansson, L. (1998) *Endocrinology* **139,** 3534–3541.
9. Papaccio, G., Pisanti, F. A., Di Montefiano, R., Graziano, A. & Latronico, M. V. G. (2002) *J. Cell. Biochem.* **86,** 651–664.
10. Bogdanov, A. A. Jr., Lewin, M. & Weissleder, R. (1999) *Adv. Drug Delivery Rev.* **37,** 279–293.
11. Larson, D. R., Zipfel, W. R., Williams, R. M., Clark, S. W., Bruchez, M. P., Wise, F. W. & Webb, W. W. (2003) *Science* **300,** 1434–1436.
12. Bremer, C., Mustafa, M., Bogdanov, A., Jr., Ntziachristos, V., Petrovsky, A. & Weissleder, R. (2003) *Radiology (Easton, Pa.)* **226,** 214–220.
13. Weissleder, R. (2001) *Nat. Biotechnol.* **19,** 316–317.
14. Harisinghani, M. G., Barentsz, J., Hahn, P. F., Deserno, W. M., Tabatabaei, S., Hulsbergen van de Kaa, C., de la Rosette, J. & Weissleder, R. (2003) *N. Engl. J. Med.* **348,** 2491–2499.
15. Josephson, L., Tung, C. H., Moore, A. & Weissleder, R. (1999) *Bioconjugate Chem.* **10,** 186–191.
16. Weissleder, R., Elizondo, G., Wittenberg, J., Rabito, C. A., Bengele, H. H. & Josephson, L. (1990) *Radiology (Easton, Pa.)* **175,** 489–493.
17. Shen, T., Weissleder, R., Papisov, M., Bogdanov, A., Jr., & Brady, T. J. (1993) *Magn. Reson. Med.* **29,** 599–604.
18. Katz, J. D., Wang, B., Haskins, K., Benoist, C. & Mathis, D. (1993) *Cell* **74,** 1089–1100.
19. Gonzalez, A., Katz, J. D., Mattei, M. G., Kikutani, H., Benoist, C. & Mathis, D. (1997) *Immunity* **7,** 873–883.
20. Weissleder, R., Heautot, J. F., Schaffer, B. K., Nossif, N., Papisov, M. I., Bogdanov, A. Jr., & Brady, T. J. (1994) *Radiology (Easton, Pa.)* **191,** 225–230.
21. Henderson, J. R. & Moss, M. C. (1985) *Q. J. Exp. Physiol.* **70,** 347–356.
22. Moore, A., Marecos, E., Bogdanov, A. Jr., & Weissleder, R. (2000) *Radiology (Easton, Pa.)* **214,** 568–574.
23. Luhder, F., Höglund, P., Allison, J. P., Benoist, C. & Mathis, D. (1998) *J. Exp. Med.* **187,** 427–432.
24. Mills, A. N. & Haworth, S. G. (1991) *J. Thorac. Cardiovasc. Surg.* **101,** 909–916.
25. Böhme, J., Schuhbaur, B., Kanagawa, O., Benoist, C. & Mathis, D. (1990) *Science* **249,** 293–295.
26. Gonzalez, A., Andre-Schmutz, I., Carnaud, C., Mathis, D. & Benoist, C. (2001) *Nat. Immunol.* **2,** 1117–1125.
27. Jansen, A., Homo-Delarche, F., Hooijkaas, H., Leenen, P. J., Dardenne, M. & Drexhage, H. A. (1994) *Diabetes* **43,** 667–675.
28. Shinomiya, M., Nadan, S., Shinomiya, H. & Onji, M. (2000) *Pancreas* **20,** 290–296.
29. Murata, Y., Amao, M. & Hamuro, J. (2003) *Eur. J. Immunol.* **33,** 1001–1011.
30. Rosmalen, J. G., Martin, T., Dobbs, C., Voerman, J. S., Drexhage, H. A., Haskins, K. & Leenen, P. J. (2000) *Lab. Invest.* **80,** 23–30.